Low kappa, narrow bandwidth Si_3N_4 Bragg gratings

Daryl T. Spencer,[1,*] Mike Davenport,[1] Sudharsanan Srinivasan,[1] Jacob Khurgin,[2] Paul A. Morton,[3] and John E. Bowers[1]

[1]*University of California Santa Barbara, Santa Barbara, California, 93106, USA*
[2]*Johns Hopkins University, Baltimore, Maryland, 21218, USA*
[3]*Morton Photonics Inc., West Friendship, Maryland, 21794, USA*
[*]*darylt@ece.ucsb.edu*

Abstract: We investigate three approaches to low perturbation gratings to achieve lower linewidths in filters and semiconductor lasers. The three designs, which are labeled post, sampled, and high order, are DUV lithography compatible and were fabricated on 90 nm thick Si_3N_4 strip waveguides. Reflection and transmission spectra measurements show coupling constant, kappa, values ranging from 0.23 cm^{-1} to 1.2 cm^{-1} with FWHM values of 74 pm to 116 pm. We discuss the tradeoffs between these geometries in terms of lowest linewidth, apodization, and curved waveguide layout. These results enable long cavity single mode lasers with kHz level linewidths on a monolithic platform.

OCIS codes: (130.3120) Integrated optics devices; (350.2770) Gratings; (230.7408) Wavelength filtering devices.

References and Links

1. K. O. Hill and G. Meltz, "Fiber Bragg grating technology fundamentals and overview," J. Lightwave Technol. **15**(8), 1263–1276 (1997).
2. C. T. Santis, S. T. Steger, Y. Vilenchik, A. Vasilyev, and A. Yariv, "High-coherence semiconductor lasers based on integral high-Q resonators in hybrid Si/III-V platforms," Proc. Natl. Acad. Sci. U.S.A. **111**(8), 2879–2884 (2014).
3. C. Henry, "Phase noise in semiconductor lasers," J. Lightwave Technol. **4**(3), 298–311 (1986).
4. M. Okai, M. Suzuki, T. Taniwatari, and N. Chinone, "Corrugation-pitch-modulated distributed feedback lasers with ultranarrow spectral Linewidth," Jpn. J. Appl. Phys. **33**(Part 1, No. 5A), 2563–2570 (1994).
5. L. A. Coldren, S. W. Corzine, and M. L. Masanovic, *Diode Lasers and Photonic Integrated Circuits*, 2nd ed. (John Wiley & Sons, Inc., 2012).
6. M. Poulin, Y. Painchaud, M. Aubé, S. Ayotte, C. Latrasse, G. Brochu, F. Pelletier, M. Morin, M. Guy, and J.-F. Cliche, "Ultra-narrowband fiber Bragg gratings for laser linewidth reduction and RF filtering," in *Proc. of SPIE 7579*, A. V. Kudryashov, A. H. Paxton, and V. S. Ilchenko, eds. (2010), 75791C.
7. P. A. Morton, V. Mizrahi, T. Tanbun-Ek, R. A. Logan, P. J. Lemaire, H. M. Presby, T. Erdogan, S. L. Woodward, J. E. Sipe, M. R. Phillips, A. M. Sergent, and K. W. Wecht, "Stable single mode hybrid laser with high power and narrow linewidth," Appl. Phys. Lett. **64**(20), 2634–2636 (1994).
8. W. Loh, F. J. O'Donnell, J. J. Plant, M. A. Brattain, L. J. Missaggia, and P. W. Juodawlkis, "Packaged, high-power, narrow-linewidth slab-coupled optical waveguide external cavity laser (SCOWECL)," IEEE Photonics Technol. Lett. **23**(14), 974–976 (2011).
9. M. J. R. Heck, J. F. Bauters, M. L. Davenport, D. T. Spencer, and J. E. Bowers, "Ultra-low loss waveguide platform and its integration with silicon photonics," Laser Photonics Rev. **8**(5), 667–686 (2014).
10. A. Yariv and M. Nakamura, "Periodic structures for integrated optics," IEEE J. Quantum Electron. **13**(4), 233–253 (1977).
11. Z. Chen, J. Flueckiger, X. Wang, F. Zhang, H. Yun, Z. Lu, M. Caverley, Y. Wang, N. A. F. Jaeger, and L. Chrostowski, "Spiral Bragg grating waveguides for TM mode silicon photonics," Opt. Express **23**(19), 25295–25307 (2015).
12. M. Belt, J. Bovington, R. Moreira, J. F. Bauters, M. J. R. Heck, J. S. Barton, J. E. Bowers, and D. J. Blumenthal, "Sidewall gratings in ultra-low-loss Si_3N_4 planar waveguides," Opt. Express **21**(1), 1181 (2013).
13. S. Zamek, D. T. H. Tan, M. Khajavikhan, M. Ayache, M. P. Nezhad, and Y. Fainman, "Compact chip-scale filter based on curved waveguide Bragg gratings," Opt. Lett. **35**(20), 3477–3479 (2010).
14. A. Hardy, D. F. Welch, and W. Streifer, "Analysis of second-order gratings," IEEE J. Quantum Electron. **25**(10), 2096–2105 (1989).
15. L. A. Weller-Brophy and D. G. Hall, "Analysis of waveguide gratings: application of Rouard's method," J. Opt. Soc. Am. A **2**(6), 863–871 (1985).

#248156 Received 18 Aug 2015; revised 31 Oct 2015; accepted 1 Nov 2015; published 11 Nov 2015

16. M. Belt and D. J. Blumenthal, "High temperature operation of an integrated erbium-doped DBR laser on an ultra-low-loss Si_3N_4 platform," in *Optical Fiber Communication Conference* (OSA, 2015), paper Tu2C.7.

1. Introduction

Bragg gratings have found many applications in sensors, telecommunication filters, and semiconductor lasers. Dispersion compensators and structural monitoring sensors based on silica fiber Bragg gratings have become commercially useful due to their low loss and precise control of a weak index perturbation [1]. Integrated gratings have also found uses as frequency selective mirrors for semiconductor lasers, but future ultra-low noise lasers with sub-kHz lasing linewidths and RIN levels below −160 dB/Hz require lower cavity losses to achieve a long effective cavity length and high mode selectivity [2]. The laser linewidth, Δv_{las} , is determined by the modified Schawlow-Townes formula, which shows that $\Delta v_{las} \propto (\Delta v_{cav})^2 / P_{las}$,where Δv_{cav} is the unpumped passive cavity linewidth and P_{las} is the output power [3]. Bragg gratings are important devices for reaching passive linewidths commensurate with >500k quality factors (sub-100 pm FWHM) while being readily integrated with a waveguide coupled gain element. Their single frequency nature and ability to be spatially sampled or apodized allows suppression of high order longitudinal modes in distributed Bragg reflector (DBR) and distributed feedback (DFB) lasers [4,5]. Generally, on-chip waveguide losses have limited the grating lengths to less than a few mm, and higher index perturbations to the waveguide were necessary to increase the net reflection. With a low loss waveguide platform, lower coupling constant, kappa (κ), values can be utilized to lengthen the grating, thus reducing the linewidth to the performance level of fiber Bragg gratings [6] and lasers utilizing those gratings [7,8]. These narrow bandwidths pave the way for sub-kHz lasing linewidths with monolithically integrated lasers, for instance, by coupling to Si/III-V active devices as previously demonstrated [9]. In this paper, we demonstrate extremely low κ designs in three different waveguide perturbation geometries, and show κ values ranging from 0.23 cm^{-1} to 1.2 cm^{-1}. These results are useful for grating lengths up to 100 mm on the ultra-low loss Si_3N_4 waveguide platform, and remain fully compatible with additional Si/III-V integration techniques. We also discuss the tradeoffs of these geometries in terms of lowest linewidth, apodization, and curved waveguide layouts.

2. Design of low kappa gratings

The linewidth of the Bragg grating, when designed to have its highest reflectivity, is proportional to κ as $\Delta \nu = c\kappa / \pi n_{eff}$, where n_{eff} is the effective index of the waveguide and c is the speed of light in the vacuum [10]. As such, we desire a weak κ for narrow linewidth, and a low loss waveguide of length L_g such that $\kappa L_g \approx 1$ to yield a suitably high reflection. A common way to implement weak κ gratings is by periodically varying the waveguide width [11,12]. But this approach has limits when you need such a small κ due to lithography limits that can impose errors and broadening due to random fluctuations. Therefore, we investigate three different grating concepts with 8 versions each, shown in Fig. 1a, termed "post", "sampled", and "high order", which are designed to produce similar reflectivity over a fixed length of 7.8 mm by tailoring the gap (g), mode order (m), or waveguide width difference (Δw) from a nominal waveguide width (w_o) [13,14]. We simulated a n_{eff} of 1.468 for the fundamental TE mode, yielding a period Δ of 528 nm at 1550 nm. The post gratings are designed to yield a low loss perturbation at the Bragg wavelength by placing a post of core material (250 × 264 nm) separated by g = 0.8, 1.0, 1.2, 1.4, or 1.6 μm away from a w_o of 2.8 μm and 3.0 μm. The higher order gratings operate at the 3rd or 5th order, giving them a period of 5λ/2 or 3λ/2 to dilute the overall perturbation. The width of the waveguide is varied with a triangular or square shape, and the difference in width is Δw = 0.2, 0.25, or 0.3 μm. The sampled gratings have a similar Δw, a fixed burst period (T) of 40.128 μm, and each burst contains N = 4, 8, 11, or 15 teeth that act as symmetric sidewall gratings. The sampled gratings have a similar perturbation as [12], which demonstrated κ values between 13 cm^{-1} to

#248156 Received 18 Aug 2015; revised 31 Oct 2015; accepted 1 Nov 2015; published 11 Nov 2015

310 cm^{-1}, but dilute the κ by sampling the reflection across multiple peaks. To determine the gaps required of the post gratings, we used the FIMMWAVE mode solver software and the T-matrix method discussed later to simulate perturbation levels on the order of $\Delta n_{eff} \approx 10^{-5}$, as required for κ values less than 1 cm^{-1}.

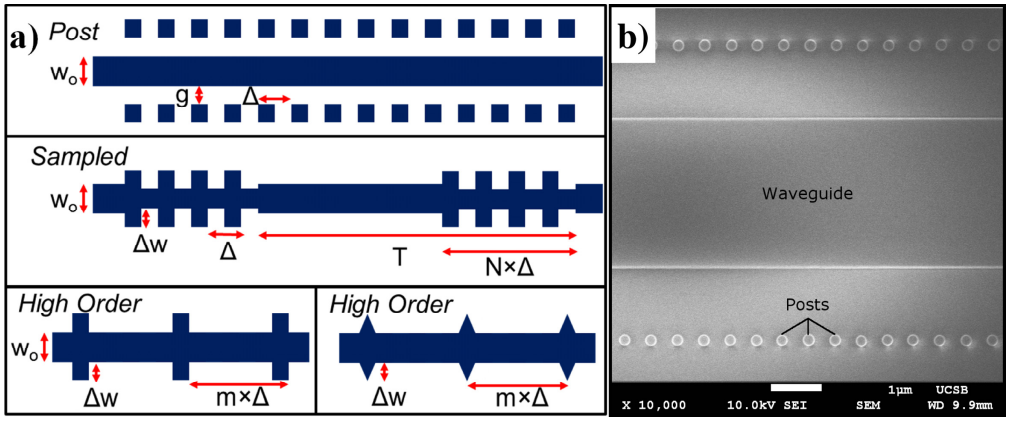

Fig. 1. a) Layout and parameter definition of the grating geometries studied in this paper. w_o: nominal waveguide width, Δ: Bragg period, g: gap, Δw: waveguide width perturbation, T: sampling period, N: number of grating periods in one sample, and m: order of the grating. b) SEM of a completed post grating device.

3. Fabrication

Fabrication begins by growing 15 μm of SiO_2 on a bare 100 mm silicon wafer by dry oxidation. The oxide is grown in batches, and is overly thick to maintain compatibility with a variety of waveguide thicknesses and waveguide confinements. In this work, a 90 nm layer of stoichiometric silicon nitride is grown by low-pressure chemical vapor deposition. Despite the high intrinsic stress of these layers, the growth techniques deposit on both sides of the wafers, which maintains wafer flatness to allow high-resolution lithography. The Si_3N_4 is patterned using a 248 nm projection lithography system. The photoresist is smoothed by a thermal reflow on a 150°C hot plate to reduce the line edge roughness of the pattern. The grating pattern and waveguide strip are both produced simultaneously in a single CMOS compatible lithography step.

Following lithography, the Si_3N_4 is etched using a $CF_4/CHF_3/O_2$ inductively coupled plasma. Removal of the photoresist is achieved with a combination of oxygen plasma ashing and photoresist stripper. The Si_3N_4 is then stripped of organic contaminants in 6:1:1 $H_2O:H_2O_2:NH_4OH$. Following cleaning, the wafer is annealed at 1050°C in a tube furnace for seven hours to drive off residual hydrogen. The upper cladding of the waveguide consists of 1.3 μm SiO_2 deposited by reactive ion sputtering. A brief *in situ* argon plasma clean is performed immediately before the deposition to ensure that the surface of the Si_3N_4 is completely clean. The sputtered film is then annealed in a rapid thermal annealer, at 800°C for 1 minute to reduce absorption. The completed wafers are separated into devices by a dicing saw and edge-polished to form facets for characterization. An SEM of a completed post grating section is shown in Fig. 1b, which shows a rounded profile due to etching, a measured period of 531 nm, and a post diameter of 227 nm.

4. Results

The completed devices were first tested for waveguide propagation loss using a 0.5 m Archimedean spiral test structure, and a Luna OBR system to monitor the backscatter versus length. Losses below 5 dB/m were achieved across the C + L bands, and <3.5 dB/m near 1550 nm. The gratings were then tested using an Agilent tunable laser, circulator, and 2 μm spot size lensed fiber. The input facet was angled at 15°, and the TE mode was excited by

#248156 Received 18 Aug 2015; revised 31 Oct 2015; accepted 1 Nov 2015; published 11 Nov 2015

optimizing the reflected power. The facet loss was measured to be 0.85 ± 0.1 dB/facet, and the TM mode did not show appreciable reflection from the gratings.

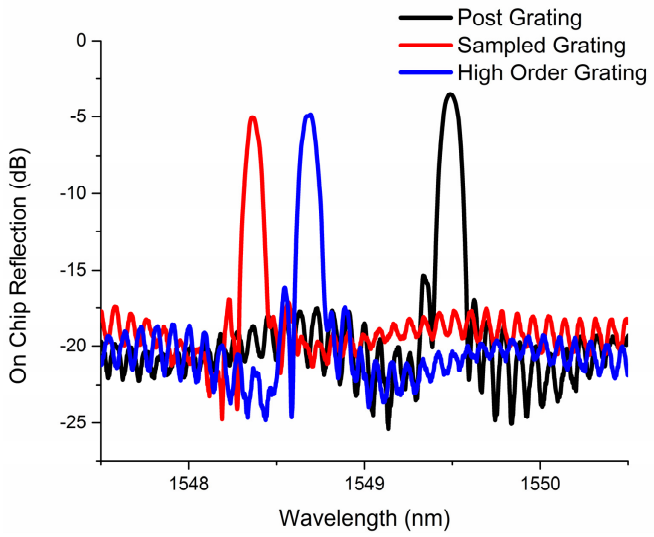

Fig. 2. Comparison of spectra for the three grating geometries. Post grating: w_o = 3.0 μm, g = 0.8 μm; sampled grating: w_o = 2.8 μm, N = 11, Δw = 0.25 μm; high order grating: w_o = 2.8 μm, m = 3, square shape, Δw = 0.2 μm.

4.1 Uniform gratings

Fig. 2 shows examples of reflection spectra from all three grating designs at similar peak reflection values. The spectra for all the grating geometries have similar features which show fairly strong Fabry-Perot resonances from the facet reflection and finite return loss of the lensed fiber (−27 dB specification). Fig. 3 shows the results of all 8 versions of the post gratings, in which the two groups correspond to the two different waveguide widths of 2.8 μm and 3.0 μm. With proper control of the gap and waveguide width, the grating reflection can be chirped or apodized in any fashion for future applications.

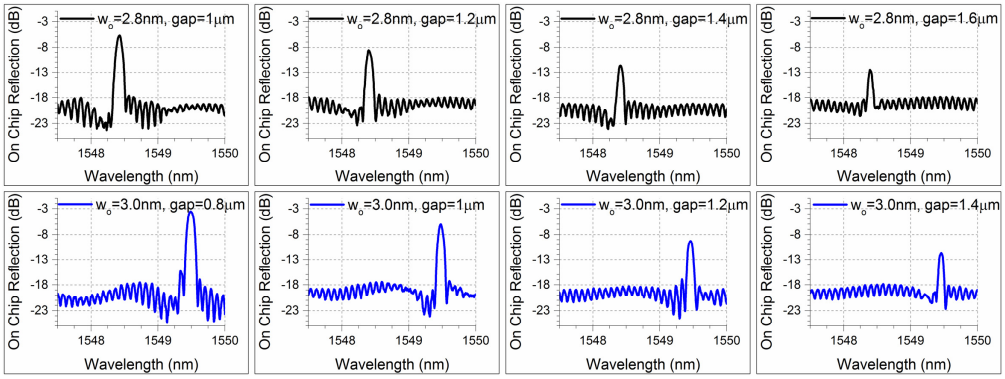

Fig. 3. Post grating spectra vs. gap for two waveguide widths.

To verify the coupling strength and FWHM, we implement a T-matrix model with an assumed plane wave interface reflectivity dependent on $\delta n = n_{eff\,2} - n_{eff\,1}$. This approach is the so-called "Rouard's Method", and facet reflections are easily implemented in the model [15]. To relate the results to the more common coupled mode theory formulation of κ [5], one must equate the net reflectivity from each half period to plane wave reflectivity to achieve

#248156 Received 18 Aug 2015; revised 31 Oct 2015; accepted 1 Nov 2015; published 11 Nov 2015

$\kappa = 2 * \delta n / \lambda_{Bragg}$. This formula equates the two theories over the entire region of interest. While this T-matrix method is useful for fitting and future grating design based on experimental data, the effective index mode solver predicted approximately 50% weaker reflections. Matching the results to simulation would require a full FDTD simulation and further understanding of the exact amount of material refractive index change during the annealing steps.

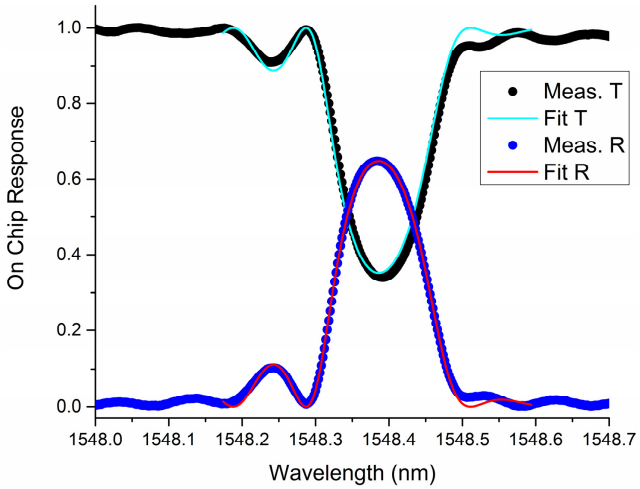

Fig. 4. Results and fit of the reflection and transmission of a sampled grating device with 15 grating teeth/burst and Δw = 0.25 μm. The asymmetries appear due to Fabry-Perot effects of the chip facets, and are accounted for in the matrix model of the gratings.

We performed a nonlinear fit to match the n_{eff} and κ values of the gratings. To show the robustness of the fits, we perform the fits on the reflection of the device, and then use these parameters to overlap with the normalized transmission spectrum. One example of this is shown in Fig. 4 for a sampled grating with 15 grating teeth/burst and Δw = 0.25 μm. Due to the non zero transmission at the grating wavelength, the output facet reflection has a small effect on the grating spectrum, which is accounted for in the fitting. Additionally, the sum of transmission and reflection in the gratings show that the excess loss is less than our measurement uncertainty of 0.5 dB. Fig. 5 and Table 1 summarize the main results of the different grating geometries, all of which achieved a κ value less than 1 cm^{-1}. It is important to note that achieving a low loss κ is the critical achievement, as higher reflection gratings for applications such as laser mirrors can be made by extending the grating length without adding appreciable propagation loss. There is a clear trend in κ and thus reflection versus gap in the post gratings and versus the number of teeth and waveguide width change Δw in the sampled gratings. The high order gratings with square perturbations also showed an increase in κ compared to triangular perturbations, due to the higher fill factor. However, the high order gratings were less controlled with waveguide width changes, possibly due to loss from coupling to radiation modes when the duty cycle is not well controlled [14]. The post gratings showed the lowest κ (0.28 cm^{-1}) and FWHM (74 pm) values, which is much improved compared to silicon-on-insulator waveguide results of κ = 90 cm^{-1} (FWHM = 1700 pm) [13] and 90 pm FWHM over 1 mm length [11]. Combined with their easier fabrication tolerance as discussed later, post gratings are the most attractive for laser mirrors and apodization profiles.

#248156 Received 18 Aug 2015; revised 31 Oct 2015; accepted 1 Nov 2015; published 11 Nov 2015

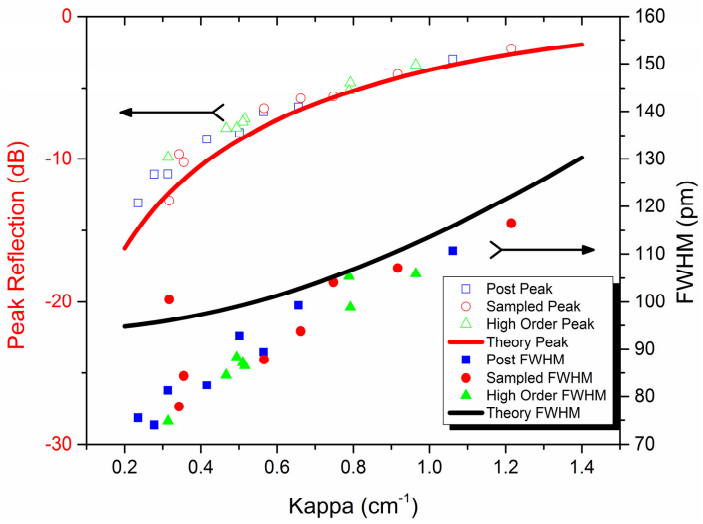

Fig. 5. Overview of the peak reflection and FWHM vs. κ values for the 7.8 mm long Bragg gratings. The measured results show slightly higher reflection and lower FWHM than ideal linear gratings due to the small amount of facet reflection.

Table 1. Results of the post, sampled, and high order gratings after removing system and facet coupling losses.

Post					Sampled					High Order				
w_o	g	κ (cm^{-1})	FWHM (pm)	Peak R (dB)	N	Δw	κ (cm^{-1})	FWHM (pm)	Peak R (dB)	Order, Shape	Δw	κ (cm^{-1})	FWHM (pm)	Peak R (dB)
2.8 µm	1.0 µm	0.66	99	–6.3	4	0.20 µm	0.32	101	–12.9	3, triangle	0.20 µm	0.47	85	–7.8
	1.2 µm	0.50	93	–8.1		0.25 µm	0.36	84	–10.2	3, square	0.20 µm	0.79	99	–4.6
	1.4 µm	0.31	81	–11.0	8	0.20 µm	0.34	78	–9.7	3, square	0.25 µm	0.96	106	–3.4
	1.6 µm	0.24	76	–13.1		0.25 µm	0.75	104	–5.6	3, square	0.30 µm	0.79	105	–5.2
3.0 µm	0.8 µm	1.06	111	–3.0	11	0.20 µm	0.57	88	–6.4	5, triangle	0.20 µm	0.31	75	–9.9
	1.0 µm	0.56	89	–6.7		0.25 µm	0.92	107	–4.0	5, square	0.20 µm	0.52	86	–7.2
	1.2 µm	0.42	82	–8.6	15	0.20 µm	0.66	94	–5.7	5, square	0.25 µm	0.49	88	–7.8
	1.4 µm	0.28	74	–11.1		0.25 µm	1.21	116	–2.3	5, square	0.30 µm	0.51	87	–7.4

4.2 λ/4-shifted gratings

While low κ Bragg gratings operating in reflection mode are one of the ways to attain narrow cavity linewidth, one can attain the same effect by using a high grating κ with a λ/4 shift operating in the transmission mode, where it would act as an integrated Fabry-Perot equivalent. In this device, the perturbation used was similar to the sampled gratings, but with a higher $\Delta w = 1.2$ µm over a 2 mm length. The measured on chip reflection and transmission spectra are shown in Fig. 6. A similar T-matrix method was used to fit the data with an average n_{eff} of 1.5709 and a transmission floor due to a finite polarization extinction ratio of 17 dB. The larger perturbation yielded a of 30 cm^{-1}, and increased the propagation loss to 20 dB/m and device insertion loss to −2.5 dB in reflection and −1.1 dB in transmission. The measured FWHM is 7.6 pm (946 MHz), with a corresponding quality factor of 204 thousand.

#248156 Received 18 Aug 2015; revised 31 Oct 2015; accepted 1 Nov 2015; published 11 Nov 2015

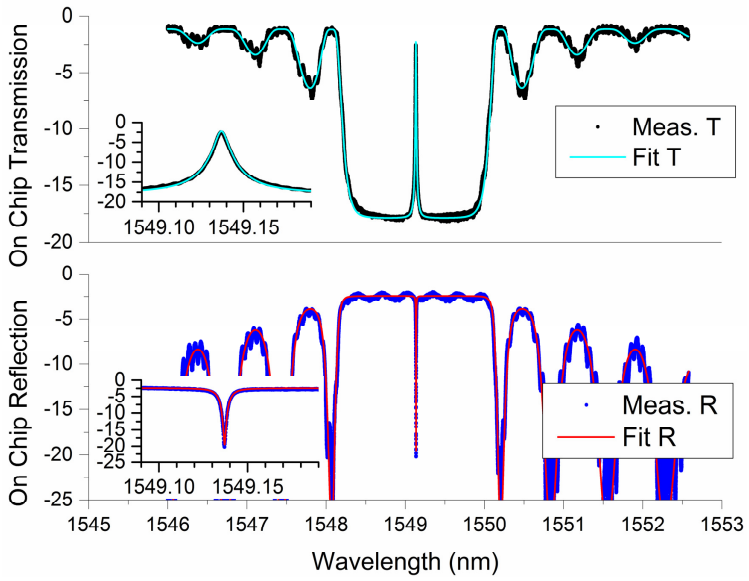

Fig. 6. Results and fit of the reflection and transmission with identical parameters for a 2 mm long grating with a λ/4-shift in the center. The transmission floor in the experiment and theory is due to a finite polarization extinction ratio, which is fit to be 17 dB.

5. Discussion

From a fabrication perspective, particularly lithography, the post grating can be advantageous for producing ultra-low κ gratings. Since the κ is well controlled by the space between the post and the waveguide, as demonstrated, very low κ can be attained without having to use a feature smaller than the 250 nm post. In principle, the κ in a post grating can be as low as desired, as opposed to the sidewall grating used on the sampled and high order gratings, which will eventually become too small to resolve.

When implementing apodization functions that vary the κ versus length, the sidewall gratings can result in less than 100 nm features that are difficult to resolve in projection lithography systems, while the post gratings are only limited by the mask writing grid which defines the gap, typically less than 5 nm for the same systems. This is most beneficial in high side mode suppression laser design and thus low RIN performance. A tradeoff occurs if curved waveguides are required for longer delays in a more compact area, such as an Archimedean spiral. In this case the effective index and thus Bragg wavelength can vary with bending radius, and sidewall gratings may be preferable to post gratings due to their proximity to the center of the waveguide. High order gratings show the least promise, as they showed little trend with Δw perturbation.

These gratings have a thin 1.3 μm top cladding and can be readily integrated with Si waveguides and hybrid Si/III-V devices through multiple wafer bonds and substrate removal of SOI and InP epitaxial material, as demonstrated in [9]. The narrow bandwidth nature of the gratings allows for >10 mm long laser cavities that are still high Q and single mode, while apodization can produce very high side mode suppression and low RIN levels. The Bragg wavelength will also shift with temperature when used with active devices, mainly be due to the thermo-optic effect, which will change the index by 10^{-5}/°C, or ≈0.01 nm/° C [16].

6. Conclusion

We have demonstrated low κ gratings for three geometries with narrow bandwidths on an ultra-low loss Si_3N_4 waveguide platform. κ values ranged from 0.23 cm^{-1} to 1.2 cm^{-1}, with bandwidths of 74 pm to 116 pm. We have also demonstrated λ/4-shifted gratings with a loaded quality factor of 204 thousand, suitable for DFB style lasers. These gratings can be

#248156 Received 18 Aug 2015; revised 31 Oct 2015; accepted 1 Nov 2015; published 11 Nov 2015

further utilized in apodization profiles, curved waveguides, or combinations such as sampled post gratings or high order post gratings. These gratings should find applications in narrow linewidth integrated lasers and narrow bandwidth filters, where the low index and ease of waveguide to waveguide coupling enables monolithic integration with Si/III-V active devices.

Acknowledgments

This research was supported by ARO under STTR Phase I contract W911NF-14-P-0021. The authors thank Wayne Chang, Michael Gerhold, and Michael Belt for helpful discussions.

#248156 Received 18 Aug 2015; revised 31 Oct 2015; accepted 1 Nov 2015; published 11 Nov 2015